

# ESP-MedSAM: Efficient Self-Prompting SAM for Universal Medical Image Segmentation

Qing Xu, Jiaxuan Li, Xiangjian He\*, *Senior Member, IEEE*, Ziyu Liu, Zhen Chen, Wenting Duan, Chenxin Li, Maggie M. He, Fiseha B. Tesema, Wooi P. Cheah, Yi Wang, Rong Qu, *Senior Member, IEEE*, Jonathan M. Garibaldi, *Fellow, IEEE*

arXiv:2407.14153v1 [eess.IV] 19 Jul 2024

**Abstract**—The Segment Anything Model (SAM) has demonstrated outstanding adaptation to medical image segmentation but still faces three major challenges. Firstly, the huge computational costs of SAM limit its real-world applicability. Secondly, SAM depends on manual annotations (e.g., points, boxes) as prompts, which are laborious and impractical in clinical scenarios. Thirdly, SAM handles all segmentation targets equally, which is suboptimal for diverse medical modalities with inherent heterogeneity. To address these issues, we propose an Efficient Self-Prompting SAM for universal medical image segmentation, named ESP-MedSAM. We devise a Multi-Modal Decoupled Knowledge Distillation (MMDKD) strategy to distil common image knowledge and domain-specific medical knowledge from the foundation model to train a lightweight image encoder and a modality controller. Further, they combine with the additionally introduced Self-Patch Prompt Generator (SPPG) and Query-Decoupled Modality Decoder (QDMD) to construct ESP-MedSAM. Specifically, SPPG aims to generate a set of patch prompts automatically and QDMD leverages a one-to-one strategy to provide an independent decoding channel for every modality. Extensive experiments indicate that ESP-MedSAM outperforms state-of-the-arts in diverse medical imaging segmentation tasks, displaying superior zero-shot learning and modality transfer ability. Especially, our framework uses only 31.4% parameters compared to SAM-Base.

**Index Terms**—Medical image segmentation, knowledge distillation, prompt engineering, lightweight network

## I. INTRODUCTION

This work is partially supported by the Yongjiang Technology Innovation Project (2022A-097-G), and the Ningbo 2025 Key R&D Project (2023Z23). (Equal contribution: Q. Xu and J. Li, \*Corresponding author: Xiangjian He)

Q. Xu, J. Li, X. He, Z. Liu, F. B. Tesema, W. P. Cheah and J. M. Garibaldi are with School of Computer Science, University of Nottingham Ningbo China, Ningbo, Zhejiang, China (e-mail: sean.he@nottingham.edu.cn).

Z. Chen is with Centre for Artificial Intelligence and Robotics (CAIR), Hong Kong Institute of Science & Innovation, Chinese Academy of Sciences, Hong Kong SAR.

W. Duan is with School of Computer Science, University of Lincoln, Lincoln LN6 7TS, UK.

C. Li is with Department of Electronic Engineering, The Chinese University of Hong Kong, Hong Kong 999077, SAR, China.

M. M. He is with Department of Cardiology, Gold Coast University Hospital, QLD, Australia.

Y. Wang is with School of Software, Dalian University of Technology, Dalian 116600, China.

R. Qu is with the School of Computer Science, University of Nottingham, Nottingham NG72RD, UK.

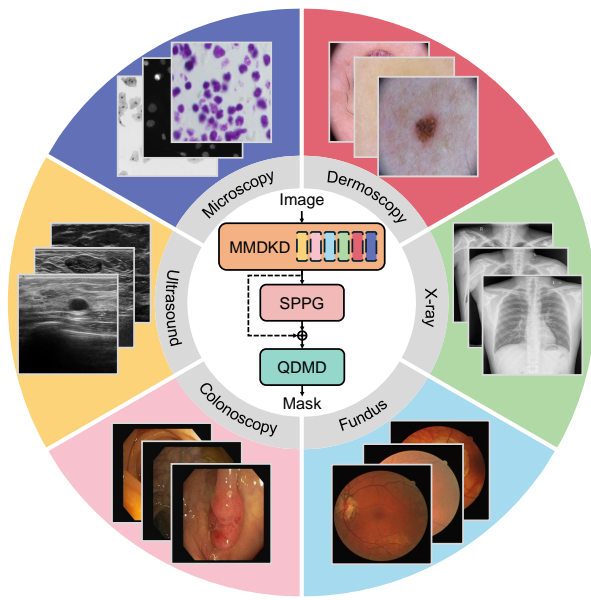


**Fig. 1.** The overview of proposed ESP-MedSAM framework for universal medical image segmentation. Our study covers various medical imaging modalities: Microscopy, Dermoscopy, X-ray, Fundus, Colonoscopy and Ultrasound.

MEDICAL imaging has made great strides in the last decades, spawning a variety of modalities, such as histopathology imaging, dermoscopy imaging, X-ray imaging, fundus imaging, colonoscopy imaging and ultrasound imaging. They play an important role in determining disease types and grading [1]. Traditionally, medical images are analysed by pathologists, which is time-consuming and occupies substantial healthcare resources. In this challenging background, computer-aided diagnosis is expected to accelerate evaluation time and improve diagnostic efficiency, where pixel-level segmentation of target regions is a key step for quantitative and qualitative assessment, presenting valuable information [2].

Convolutional Neural Network (CNN) based U-shape architectures investigate the correlation between the low-level and high-level semantic information in mask prediction [3]–[7]. With supervised learning strategies, these studies demonstrate the accurate generation of segmentation masks in a single modality [7]–[10]. However, it is difficult for these methods to handle multiple modalities of segmentation tasks simulta-

neously due to their limited receptive field. This discrepancy raises significant challenges in establishing a segmentation model with superior generalisation and accuracy across various medical images [11], [12].

Vision Transformer (ViT) [13] leverages the self-attention mechanism to capture long-range dependencies and provides a larger model capacity to increase generalisation under the supervision of big data. With these advantages, the recent appearance of Segment Anything Model (SAM) [14] has made a significant breakthrough in the field of image segmentation. The superior performance of SAM in natural images has been sufficiently validated, demonstrating its robustness and adaptability in a wide range of scenarios through prompt engineering. In medical domains, current studies [15], [16] fully fine-tune SAM to demonstrate its potential for medical image segmentation tasks across multiple modalities.

Despite these advantages, adapting SAM to clinical applications faces three significant obstacles. Firstly, the standard SAM [14] contains a large number of parameters, even SAM-Base still takes 91M parameters. This is because its image encoder is very expensive. The huge computational costs limit the applicability of SAM in real-world scenarios. Although existing methods based on Parameter-Efficient Fine-Tuning (PEFT) techniques [17]–[19] reduce training parameters, the size of the entire model is not decreased, but even increased.

Secondly, SAM [14] depends on manual annotations (e.g., points, boxes) as prompts to guide the segmentation mask generation. Although the SAM based on the bounding box prompt mode can produce relatively precise masks, it requires users to roughly provide the location of diseases in clinical cases, which can only be completed by medical experts, defeating the purpose of healthcare AI. Particularly, for the most effortless mode (i.e., point prompt), recent studies [15], [16] have indicated that it is difficult to perform acceptable results in medical applications by using only a pair of positive and negative points.

Thirdly, the original SAM [14] leverages three mask queries to predict potential segmentation masks for all classes and corresponding Intersection over Union (IoU) scores. However, in the field of medical imagining, every vision modality has inherent heterogeneity. This many-to-many strategy is difficult to harmonise the mutual knowledge interference of different modalities, resulting in the degradation of model generalisation.

To tackle the limitations of SAM, we propose an efficient self-prompting SAM framework for cross-modality medical image segmentation, named ESP-MedSAM. Specifically, we present the Multi-Modal Decoupled Knowledge Distillation (MMDKD) method to store the knowledge of each medical modality to a modality controller and transfer common image knowledge of the huge image encoder into a lightweight image encoder. The modality controller drives the lightweight image encoder to produce discriminative visual features across diverse modalities. Then, we devise the Self-Patch Prompt Generator (SPPG) to automatically produce a set of patch prompts assisting the prediction of segmentation masks. Moreover, we introduce the Query-Decoupled Modality Decoder (QDMD), applying the one-to-one strategy to personalise the

decoding process for each medical modality, preventing the different modalities from interfering with each other.

The contributions of this work are summarized as follows.

- We propose a novel MMDKD strategy to distil the common image knowledge and domain-specific medical knowledge from the foundation model to a lightweight image encoder and a modality controller respectively, leading to the reduction of computational costs while retaining the generalisation capabilities.
- We devise the SPPG to produce high-quality patch prompts automatically without the demand for manual annotations. These prompts are used to guide the prediction of segmentation masks.
- We introduce the QDMD for the segmentation decoding. It leverages the decoupled one-to-one strategy to provide a private segmentation workflow to each modality, preventing the different modalities from interfering with each other.
- We take the lightweight image encoder and modality controller distilled by MMDKD, SPPG and QDMD to build our ESP-MedSAM with remarkable generalisation-efficiency trade-offs. We conduct extensive experiments on diverse medical imaging modalities, proving that our ESP-MedSAM outperforms state-of-the-art (SOTA) SAM-based architectures, especially for nuclei image and fundus vessel segmentation tasks.

## II. RELATED WORK

### A. SAM for Medical Image Segmentation

Segment Anything Model (SAM) [14] has achieved remarkable success in field image segmentation across diverse scenarios. It comprises three modules: a large ViT encoder for feature extraction, a prompt encoder that utilises manual input points, boxes, texts, or low-resolution masks to assist segmentation decoding and a mask decoder for mask prediction. Taking advantage of the 11M training images, SAM reveals outstanding zero-shot generalisation in various natural image segmentation tasks. In medical domains, MedSAM [16] and SAMMI [15] collected more than 1M public medical images to fully fine-tune SAM with box and point prompts for medical image segmentation. However, such methods rapidly increase data and computation costs, which are expensive and impractical in clinical scenarios. To mitigate the reliance on data size and computational resources in transfer learning, parameter-efficient fine-tuning techniques have been introduced in SAM. Specifically, Adapter [20] has been widely used to integrate into the image encoder of SAM for the refinement of feature representation in medical imaging [17], [18], [21]. SAMed [19] concatenated Low-Rank Adaptation (LoRA) [22] with self-attention layers of SAM to guide the feature extraction. Zhong *et al.* [23] proposed Conv-LoRA that incorporates multiple parallel convolutional experts with LoRA to sample different feature scales. These SAM-based architectures, while beneficial, handle all modalities equally, making it difficult to prevent mutual interference between different modalities and to generalise them to other unseen domains. In contrast, our

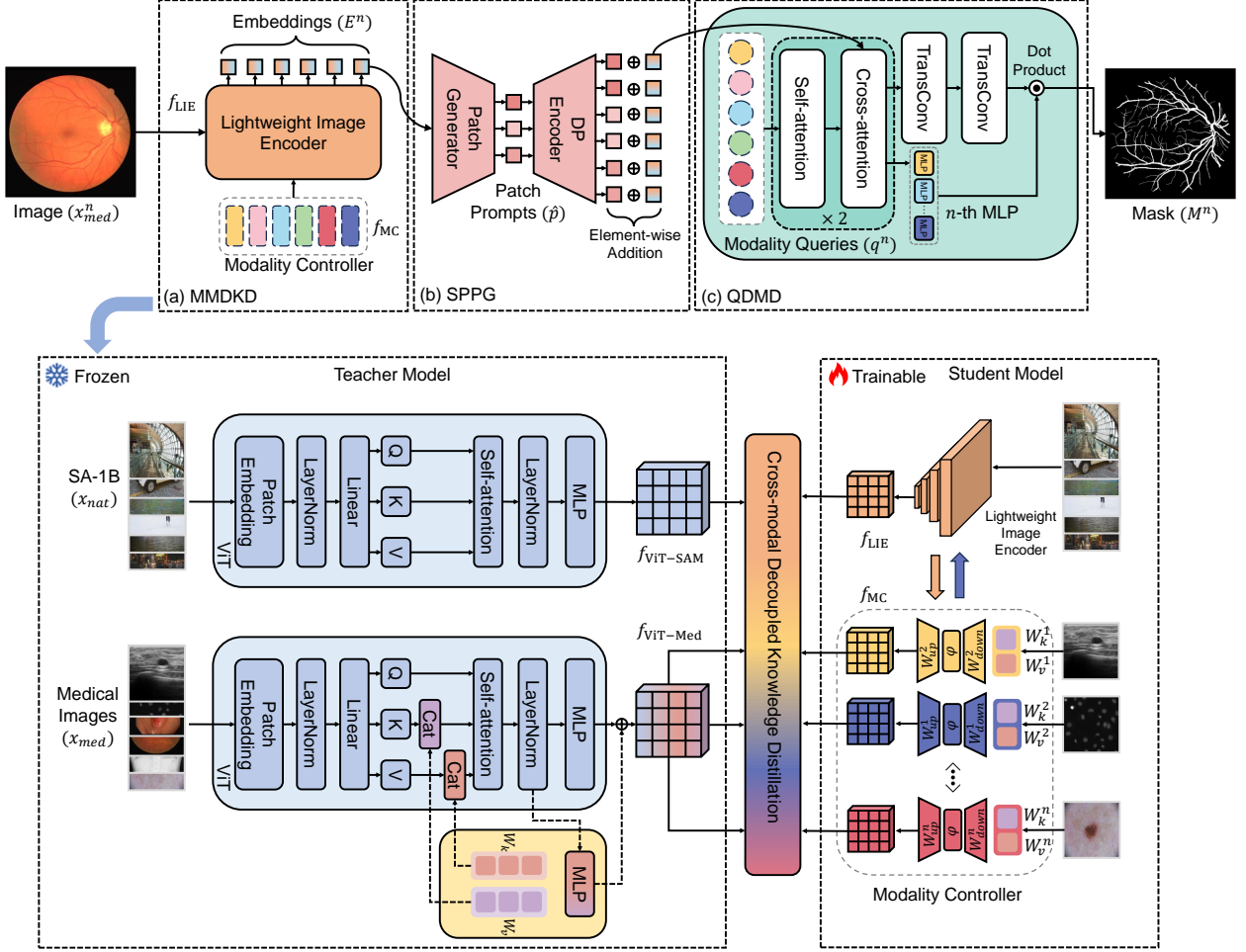


**Fig. 2.** The end-to-end architecture of our ESP-MedSAM for universal medical image segmentation. (a) Multi-Modal Decoupled Knowledge Distillation. (b) Self-Patch Prompt Generator. (c) Query-Decoupled Modality Decoder.

approach overcomes this specific limitation and illustrates superior generalisation across a variety of nuclei image domains.

Furthermore, the reliance on laborious manual annotations as segmentation prompts seriously reduces their applicability in clinical scenarios. Although the standard SAM provides a simple sliding window algorithm to automatically generate box and centre point prompts from inputs, recent studies [15], [24] have indicated this approach fails to perform satisfactory results in medical image segmentation tasks. To minimise the need for manual annotations, SPPNet [25] computed neighbouring points around the centroid as prompts for nuclei image segmentation. Traditional segmentation networks (e.g., UNet [3]) are considered to produce low-resolution masks as prompts to provide for their mask decoders [26]–[28]. However, such pixel-level segmentors may generate more prediction errors when facing diverse vision modalities due to their limited capacities. Instead of a dual-branch architecture, our ESP-MedSAM framework extracts a set of patch prompts from its own image embeddings for guiding segmentation decoding, which retains the generalisation performance across multiple modalities without demanding labour-intensive manual annotations.

### B. Knowledge Distillation

Knowledge Distillation (KD) [29] is a method of compressing the size of models, transferring the knowledge from the teacher model to the student model. Generally, hard labels (e.g., category) and soft labels (e.g., probability) are used to supervise the learning of a student model from a teacher model. Yang *et al.* [30] decoupled the distillation into two stages: representation learning and classification. Subsequently, decoupled knowledge distillation [31] was introduced to divide the traditional KD loss into two parts: target class and non-target class knowledge distillation, which enhances the efficiency of knowledge transfer between the teacher and student model. In addition, it has been proven that soft labels are preferable in KD-based medical image segmentation [32]–[34]. Recently, transferring the knowledge of SAM to a small model has become a hot research topic. MobileSAM [35] retained the prompt encoder and mask decoder of the standard SAM [14], adopting feature distillation between its image encoder and the TinyViT [36]. EdgeSAM [37] involved both the prompt encoder and mask decoder in the distillation process to capture the full knowledge embodied in SAM. EfficientSAM [38] utilised masked image pretraining method and reconstruction loss to transfer the knowledge from the

image encoder of SAM to a lightweight encoder. However, these feature-coupled distillation methods are challenging to harmonise the feature representation across diverse modalities with inherent heterogeneity, resulting in the degradation of the model generalisation capability. On the contrary, our MMDKD strategy uses independent feature distillation for each modality, enabling the generation of discriminative features for different medical modalities.

### III. METHODOLOGY

#### A. Overview of *ESP-MedSAM*

As presented in Fig. 2, we illustrate our *ESP-MedSAM* architecture for universal medical image segmentation across various modalities. Given medical images from the  $n$ -th modality from the total  $N$  modalities, we first utilise a modality controller to boost a lightweight image encoder in generating a set of discriminative image embeddings. Both modules are distilled from the large ViT-based teacher model using the MMDKD strategy. Then, these embeddings are delivered to the SPPG module, which is automatically converted to a set of patch prompts to assist segmentation decoding. Finally, QDMD leverages the independent query of the corresponding modality to customise the decoding process for individual medical modalities.

Overall, MMDKD significantly reduces the computational costs of feature extraction. SPPG eliminates the requirement of manual annotations in prompt generation. QDMD prevents different modalities from interfering with each other when predicting segmentation masks.

#### B. Multi-Modal Decoupled Knowledge Distillation

The key obstacle of SAM [14] is the large ViT and huge computation costs which limit its applications in real-world scenarios. Recent studies [35], [37]–[41] mainly aim to transfer the knowledge of ViT into a lightweight image encoder. However, in the field of medical imaging, different modalities face inherent heterogeneity. With the reduction of model capacity, single image encoders is difficult to harmonise the feature representation of the model across diverse modalities, thereby degrading the model generalisation. To address the aforementioned challenge, we propose the MMDKD to transfer common image knowledge and domain-specific medical knowledge of the foundation model into a lightweight image encoder and a modality controller respectively, which is presented in Fig. 2a. The modality controller drives the lightweight image encoder to generate discriminative features for different modalities.

1) *Structure of Multi-Modal Teacher Model*: To conduct the distillation process, we first construct a multi-modal teacher model that involves the natural image encoder  $f_{ViT-SAM}$  of SAM [14] and a medical image encoder  $f_{ViT-Med}$  that is acquired by fine-tuned SAM. Specifically, inspired by PEFT techniques, we freeze the image encoder of SAM and train a small number of trainable parameters to adapt the feature representation of various medical images. In detail, a set of dynamic tokens  $\{W_k, W_v\}$ , is concatenated with the *key* and *value* channels of the multi-head attention layer, adaptively

adjusting attention to learn new pattern from medical image patches. Then, we add another Multi-Layer Perceptron (MLP) layer to expand the model capacity. We fine-tune this SAM on diverse medical vision modalities. As a result,  $f_{ViT-SAM}$  and  $f_{ViT-Med}$  are used to provide common image knowledge and domain-specific medical knowledge respectively.

2) *Decoupled Knowledge Distillation*: The primary challenge in performing KD from foundation models to lightweight frameworks is selecting reliable labels as supervisions to optimise the learning of the student model. Intuitively, the quality of segmentation masks depends on the feature extracted from the image encoder. Drawing inspiration from the divide-and-conquer algorithm, our proposed MMDKD method decouples the KD process into two sub-tasks: universal feature distillation and modality-specific feature distillation. We first transfer the knowledge from  $f_{ViT-SAM}$  to a lightweight image encoder  $f_{LIE}$ , e.g., TinyViT [36]. Secondly, we extract the specific knowledge of each medical modality from  $f_{ViT-Med}$ , and store it in a separate set of parameter bags  $\{W_k^n, W_v^n, W_{down}^n, W_{up}^n\}$ , where  $n \in 1, 2, \dots, N$ ,  $W_k^n$  and  $W_v^n$  are the decoupled tokens corresponding to the  $n$ -th modality, and  $W_{down}^n$  and  $W_{up}^n$  are two fully connected layers. All parameter bags constitute a modality controller  $f_{MC}$ . The loss function of optimising these two modules is defined by:

$$L_{MMDKD} = \left\| f_{ViT-SAM}(x_{\text{nat}}) - f_{LIE}(x_{\text{nat}}) \right\|_2^2 + \sum_{n=1}^N \left\| f_{ViT-Med}(x_{\text{med}}^n) - f_{MC}(x_{\text{med}}^n) \right\|_2^2, \quad (1)$$

where  $x_{\text{nat}}$  stands for the natural image collected from the SA-1B dataset [14] and  $x_{\text{med}}$  is the medical image collected from six medical datasets with different modalities. The MMDKD strategy provides a modular image encoder for personalising the feature representation of different medical imaging modalities, preventing different modalities from interfering with each other.

3) *Modularised Feature Generation*: Given a medical image from the  $n$ -th modality (for  $n = 1, 2, \dots, N$ ),  $f_{MC}$  sequentially connect the parameter bag  $\Phi^n$  of each modality to  $f_{LIE}$ . Similar to the teacher model  $f_{ViT-Med}$ ,  $\{W_k^n, W_v^n\}$  concatenates with the key and value branch of  $f_{LIE}$  to conduct more effective attention computation:

$$E^n = \text{softmax}\left(\frac{Q \cdot (K \frown W_k^n)^T}{\sqrt{d}}\right) \cdot (V \frown W_v^n), \quad (2)$$

where  $E^n$  is a set of image embeddings,  $\frown$  is the concatenation operation.  $Q$ ,  $K$  and  $V$  are weight vectors in  $f_{LIE}$ ,  $d$  stands for dimensions and  $\cdot$  is the matrix multiplication. Finally, we parallel our  $\{W_{down}^n, W_{up}^n\}$  with the MLP  $\Phi$  in  $f_{LIE}$  to capture new information from embeddings:

$$E^n \leftarrow E^n + \Phi(E^n) + \varphi(E^n \cdot W_{down}^n)W_{up}^n, \quad (3)$$

where  $\varphi$  is a nonlinear activation function (e.g., GELU). Overall, our proposed MMDKD method efficiently decreases the computational costs of feature extraction.

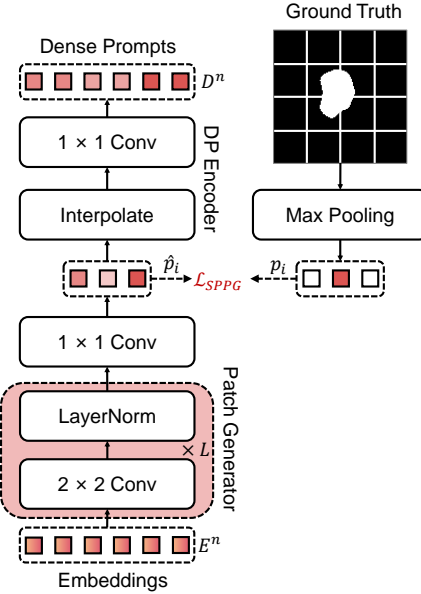


Fig. 3. The illustration of Self-Patch Prompt Generator.

### C. Self-Patch Prompt Generator

Current medical SAM [15], [16], [18], [19] and lightweight SAM [35], [37]–[41] mainly leverage manual prompts (e.g., points and boxes) to guide the model providing satisfied segmentation masks. However, such methods rely on the experience of pathologists in medical scenarios, which are expensive and time-consuming. To eliminate the demand for manual annotations, we propose the SPPG that contains a patch generator and Dense Prompt (DP) encoder to automatically produce a set of high-quality patch prompts to assist segmentation decoding. As presented in Fig. 3, the patch generator  $\delta$  consists of  $L$  convolutional layers for patch merging and  $1 \times 1$  convolution for channel compression, where each layer includes  $2 \times 2$  convolution with stride 2 followed by LayerNorm. As the image embedding  $E^n$  contains rich semantic information, we consider it as the input. The default patch size is the same as that (i.e., 16) of the standard SAM [14]. With each additional convolutional layer, the scale of the patch is doubled. The prediction of patch prompts  $\hat{p}_n$  can be formulated as:

$$\hat{p}_n = \frac{1}{1 + e^{-(\delta(E^n))}}. \quad (4)$$

The reason for adopting patch prompts is that the target area of many medical images is much smaller than the background. The patch prompt is essentially an inductive prediction, reducing the complexity of predicting the final segmentation mask by providing the summarized semantic information to the decoder. To optimise the generated patch prompts, we utilise binary cross-entropy loss to perform computation:

$$L_{SPPG} = -\frac{1}{N} \sum_{n=1}^N p_n \log(\hat{p}_n) + (1 - p_n) \log(1 - \hat{p}_n), \quad (5)$$

where  $p_n$  is the target patch generated by maxpooling the ground truth of  $n$ -th modality. We then respectively use the interpolation method for upsampling  $\hat{p}_n$  and  $1 \times 1$  convolution

to align the dimension with the image embedding  $E^n$ . They constitute the DP encoder. In this way, the SPPG module automatically produces a set of high-quality dense prompts  $D^n$  to guide the prediction of segmentation masks, improving the applicability of ESP-MedSAM in clinical scenarios.

### D. Query-Decoupled Modality Decoder

The mask decoder of SAM [14] utilises one query token to handle the single-level segmentation task in natural images. However, this is not optimal for medical image segmentation. As there exists inherent heterogeneity in various medical imaging modalities, it is likely for the modalities to interfere with each other and degrade the model performance. To prevent interference, we propose the QDMD for our ESP-MedSAM framework, as provided in Fig. 2c. Concretely, we set  $N$  query tokens  $\{q^1, q^2, \dots, q^N\}$  to customize the private workflow for each Modality. We adopt a class-fixed assign algorithm, and each query token corresponds to one modality category. Given the image embeddings  $E^n$  and prompt embeddings  $D^n$ , we first fuse them by an element-wise addition operation  $\oplus$  and conduct cross-attention with the query token  $q^n$ :

$$F^n = \text{softmax}\left(\frac{((E^n \oplus D^n) + \alpha) \cdot f_{SA}(q^n)^T}{\sqrt{d}}\right) \cdot f_{SA}(q^n) + (E^n \oplus D^n), \quad (6)$$

where  $F^n$  is the updated fusion embedding of  $n$ -th modality,  $\alpha$  stands for the corresponding positional encodings and  $f_{SA}$  is a self-attention layer. Similar to SAM [14], such operations are iterated twice. To predict the segmentation mask  $M^n$ , we perform:

$$M^n = \sigma(\Psi(F^n) \cdot f_{MLP}^n(f_{SA}(q^n))), \quad (7)$$

where  $\Psi$  represents two  $2 \times 2$  transpose convolutions, upsampling  $F^n$  by  $2 \times$ .  $n$ -th MLP aligns the channel with upscaled  $F^n$  and contains the decoding information of corresponding modalities.  $\sigma$  stands for a sigmoid operation followed by an interpolation function that recovers the size of masks.  $M^n$  is supervised by a combination of focal loss and dice loss:

$$L_{\text{Mask}} = \lambda L_{\text{focal}} + L_{\text{dice}}, \quad (8)$$

where  $\lambda$  represents the coefficient to adjust the weight of focal loss. Consequently, the proposed QDMD provides an independent decoding process for each modality, which avoids the conflicting inherent heterogeneity of different modalities, improving the model generalisation performance.

## IV. EXPERIMENTS

### A. Datasets and Implementations

1) *Datasets*: To validate the effectiveness of our proposed ESP-MedSAM, we select various 2D medical imaging modalities: Dermoscopy, X-ray, Fundus, Colonoscopy, Ultrasound and Microscopy. Each modality contains one dataset. In addition, we test the zero-shot generalisation of our model on STARE [43] and evaluate the transfer ability on the Histopathology modality. The details are as follows.

TABLE I  
COMPARISON WITH STATE-OF-THE-ART LIGHTWEIGHT SAM FRAMEWORKS IN MEDICAL IMAGE SEGMENTATION.

Methods	Manual Prompt	Dermoscopy		X-ray		Fundus		Colonoscopy		Ultrasound		Microscopy	
		Dice $\uparrow$	HD $\downarrow$										
MobileSAM [35]	Point	87.97	105.34	96.25	50.94	69.31	94.41	81.83	86.46	66.48	107.78	87.42	131.00
RepViT-SAM [39]		88.00	106.75	96.07	52.71	67.76	98.66	81.81	154.65	68.38	103.09	88.81	127.17
EfficientViT-SAM-L0 [40]		88.49	103.61	96.43	49.07	70.98	91.16	85.16	102.72	74.71	113.18	89.37	116.42
EfficientSAM-S [38]		87.11	108.12	96.40	49.77	70.09	89.27	82.81	96.35	71.17	113.57	88.41	129.08
EdgeSAM [37]		88.10	100.92	96.18	51.60	68.04	92.40	81.76	105.06	67.64	105.51	87.35	113.46
SAM-Lightening [41]		88.28	101.64	96.41	50.35	69.72	95.74	83.70	97.79	73.07	129.53	89.18	111.67
MobileSAM [35]	x	86.19	168.48	94.75	175.50	25.56	254.24	77.29	284.32	61.51	342.22	61.49	307.44
RepViT-SAM [39]		85.73	157.66	94.27	170.27	25.10	263.76	78.75	296.36	61.62	440.75	60.54	287.63
EfficientViT-SAM-L0 [40]		87.18	151.29	96.13	128.60	25.95	252.39	82.48	317.51	65.44	354.98	66.32	292.69
EfficientSAM-S [38]		87.02	162.45	94.89	169.20	25.84	261.51	78.54	305.36	62.05	430.18	60.56	336.55
EdgeSAM [37]		85.86	153.97	94.52	183.37	25.62	257.85	76.41	328.79	60.24	400.69	59.68	357.20
SAM-Lightening [41]		86.99	165.80	95.83	115.19	25.52	261.25	80.14	292.33	62.59	376.55	62.68	306.66
ESP-MedSAM-S	x	<b>88.89</b>	<b>98.71</b>	<b>96.57</b>	<b>48.50</b>	<b>72.55</b>	<b>71.99</b>	<b>92.84</b>	<b>49.42</b>	<b>77.86</b>	<b>80.25</b>	<b>89.70</b>	<b>93.26</b>

TABLE II  
COMPARISON WITH PEFT SAM FRAMEWORKS IN MEDICAL IMAGE SEGMENTATION.

Methods	Manual Prompt	Dermoscopy		X-ray		Fundus		Colonoscopy		Ultrasound		Microscopy	
		Dice $\uparrow$	HD $\downarrow$										
SAM [14]	Point	85.87	141.29	95.77	83.24	78.16	72.22	80.56	83.24	78.50	115.10	89.64	154.13
SAMMI [15]		85.49	165.10	95.96	77.19	56.05	171.46	78.28	158.95	75.37	137.99	85.21	134.58
MedSAM [16]		85.81	147.19	96.15	106.49	57.26	150.68	79.97	147.13	75.99	128.01	84.93	126.41
SAMUS [17]		87.93	102.07	96.54	53.03	79.07	67.09	89.66	93.55	73.62	166.86	91.53	131.85
Med-SA [18]		88.86	99.75	96.32	50.74	78.09	68.02	90.08	91.79	77.30	104.72	91.00	115.87
SAMed [19]		87.03	131.46	96.58	52.25	79.69	65.01	89.79	119.92	82.19	110.70	90.85	117.53
SAM-CL [42]		88.31	99.08	96.19	49.52	79.51	62.65	91.56	82.28	77.29	121.73	90.88	116.17
UV-SAM [26]	x	87.42	126.23	95.85	58.24	70.39	79.09	78.39	115.50	58.84	115.24	89.97	132.26
LeSAM [28]		88.63	98.12	96.10	52.79	75.12	75.77	85.92	82.16	74.62	122.20	90.35	128.09
H-SAM [27]		87.84	103.79	96.57	54.70	77.47	69.83	87.82	97.80	74.59	110.71	90.81	124.34
ESP-MedSAM-T	x	<b>89.07</b>	<b>95.07</b>	<b>96.64</b>	<b>46.39</b>	<b>80.93</b>	<b>58.29</b>	<b>93.14</b>	<b>44.09</b>	<b>88.08</b>	<b>76.13</b>	<b>92.03</b>	<b>92.61</b>

TABLE III

COMPARISON WITH COMPUTATION COSTS IN THE AUTOMATIC MASK GENERATION MODE.

Method	Params $\downarrow$	FLOPs $\downarrow$	FPS $\uparrow$
MobileSAM [35]	9.79M	39.71	1.05
RepViT-SAM [39]	9.57M	23.64	1.12
EfficientViT-SAM-L0 [40]	34.80M	89.10	0.91
EfficientSAM-S [38]	25.38M	32.51	0.98
EdgeSAM [37]	9.60M	22.10	1.25
SAM-Lightening [41]	19.26M	52.46	1.02
ESP-MedSAM-S	28.46M	55.86	12.87

**Dermoscopy:** ISIC-2018 [44], [45], hosted at the Medical Image Computing and Computer Assisted Intervention (MICCAI) conference, is a skin lesion segmentation dataset towards melanoma detection, including 3694 annotated images.

**X-ray:** Montgomery County CXR Set [46], [47] is a lung segmentation dataset for abnormal detection with manifestations of tuberculosis, including effusions and military patterns. The set covers 563 images.

**Fundus:** DRIVE [48] dataset is applied for vessel segmentation in digital retinal images. It involves 40 pixel-level labelled images from diabetic patients between 25 and 90 years of age. STARE [43] dataset contains 20 manually labelled images for diagnosing retinal disease, e.g., central retinal artery occlusion.

**Colonoscopy:** CVC-ClinicDB [49] is a polyp segmentation dataset collected from 31 colonoscopy sequences. There are 612 slides extracted from these colonoscopy videos.

**Ultrasound:** UDIAT [50] dataset is used for breast ultrasound lesions detection. It contains 163 images from different women with cancerous masses and benign lesions.

**Microscopy:** 2018 Data Science Bowl [51] is a nuclei image segmentation dataset. It includes 670 microscopic images with different cell lines, staining protocols and imaging conditions.

**Histopathology:** TNBC [52] contains 50 histopathology images at  $40\times$  magnification for the nuclei segmentation task. It was collected from triple-negative breast cancer patients.

**2) Implementation Details:** We perform all experiments on a single NVIDIA A6000 GPU with PyTorch. We perform the optimiser using Adam with a learning rate of  $1 \times 10^{-4}$ . The batch size and epochs are set to 4 and 200, respectively. We apply the exponential decay strategy to adjust the learning rate. All images are resized to  $1024 \times 1024$  during the training and test stages. we set the patch size as 32 in the SPPG, i.e.,  $L = 1$ . In the comparison of lightweight frameworks, MobileSAM [35], RepViT-SAM [39], EfficientViT-SAM-L0 [40], EfficientSAM-Ti [38], EdgeSAM [37] and SAM-Lightening [41] serving as baselines. In addition to testing the manual point mode, they perform the automatic mask generation mode [14]. To save the memory in the stage of fine-tuning the standard SAM, we use ViT-B [13] as the teacher image

TABLE IV  
ZERO-SHOT GENERALIZATION COMPARISON ON STARE.

Methods	Manual Prompt	Dice $\uparrow$	HD $\downarrow$
SAM [14]		63.21	148.98
SAMMI [15]		32.74	217.26
MedSAM [16]		33.12	235.26
SAMUS [17]	Point	75.06	108.25
Med-SA [18]		74.31	120.07
SAMed [37]		75.24	95.63
SAM-CL [42]		75.11	123.79
UV-SAM [18]		69.13	132.99
LeSAM [37]	<b>x</b>	70.85	99.71
H-SAM [42]		72.14	96.86
ESP-MedSAM-T	<b>x</b>	<b>76.89</b>	<b>86.32</b>
MobileSAM [35]		69.67	109.69
RepViT-SAM [39]		67.38	98.85
EfficientViT-SAM-L0 [40]	Point	70.11	108.25
EfficientSAM-Ti [38]		69.89	110.33
EdgeSAM [37]		69.20	98.04
SAM-Lightening [41]		68.38	117.23
ESP-MedSAM-S	<b>x</b>	<b>71.25</b>	<b>88.00</b>

TABLE V  
TRANSFER ABILITY COMPARISON ON HISTOPATHOLOGY.

Methods	Manual Prompt	Dice $\uparrow$	HD $\downarrow$
MobileSAM [35]		81.04	139.30
RepViT-SAM [39]		79.46	143.26
EfficientViT-SAM-L0 [40]	Point	82.22	128.76
EfficientSAM-Ti [38]		81.13	140.64
EdgeSAM [37]		81.27	136.39
SAM-Lightening [41]		81.54	131.52
U-Net [3]		80.83	145.57
nnUNet [6]	<b>x</b>	82.11	122.32
TransUNet [53]		81.24	147.11
ACC-UNet [54]		81.85	146.34
ESP-MedSAM-S	<b>x</b>	<b>83.14</b>	<b>111.83</b>

encoder. In the comparison of PEFT and end-to-end SAM variants, we select SAMUS [17], Med-SA [18], SAMed [19], SAM-CL [42], UV-SAM [26], LeSAM [28] and H-SAM [27] as baselines, with the same encoder size and training configurations. We also fine-tune the prompt encoder and mask decoder of SAM [14], SAMMI [15] and MedSAM [16]. These architectures are trained with the point prompt mode [14] that uses the *ConnectedComponentsWithStats* function in OpenCV to calculate the centroid of each instance as point prompts.

**3) Evaluation Metrics:** To perform the comprehensive evaluation of medical image segmentation, we adopt two common metrics: Dice coefficient and Hausdorff Distance (HD). Both measure the similarity between the prediction and Ground Truth (GT), where HD is more sensitive to the boundary than Dice. We also report model parameters, Floating Point Operations (FLOPs), Frames Per Second (FPS) and GPU Memory to reveal the computation costs. To match the predicted  $N$  masks with the corresponding ground truth  $G$ , we calculate the Dice score between each mask  $M^n$  and  $G$ . The one with the highest Dice score in this set is chosen as the matching prediction mask for the following evaluation of segmentation

TABLE VI  
ABLATION STUDY OF ESP-MEDSAM IN MEDICAL IMAGE SEGMENTATION.

Row	MMDKD	SPPG	QDMD	Dice (Avg.) $\uparrow$	HD (Avg.) $\downarrow$	Params $\downarrow$
1				84.75	108.20	90.58M
2	✓			85.56	92.16	29.08M
3		✓		84.91	76.99	90.60M
4			✓	85.28	91.37	89.94M
5	✓	✓		86.26	75.18	29.10M
6	✓		✓	85.93	90.93	28.44M
7		✓	✓	85.61	76.31	89.96M
8	✓	✓	✓	<b>86.70</b>	<b>73.69</b>	28.46M

[15].

### B. Comparison with State-of-the-Art Lightweight SAMs

To validate the effectiveness of our lightweight ESP-MedSAM-S framework in medical instance segmentation, we compare with SOTA lightweight SAM architectures [35], [37]–[41] on six 2D medical imaging modalities, as illustrated in Table I. For fair comparisons, the knowledge of these student models is distilled from the same ESP-MedSAM-T teacher model in Table II. It can be observed that the proposed ESP-MedSAM outperforms other lightweight SAMs in all six modalities, even using the manual point input as the prompt. Particularly, with the automatic mask generation mode, the performance of state-of-the-arts in retinal vessel and nuclei segmentation tasks declines rapidly. In contrast, ESP-MedSAM-S surpasses these models with a 46.6% to 47.45% and 23.38% to 30.02% Dice increase, respectively. On HD metric, our ESP-MedSAM framework reduces the distance by up to 6.5 $\times$  compared to current SOTA models. Furthermore, we compare the computation costs of the automatic mask generation in Table III. We observe that the proposed ESP-MedSAM-S performs faster inference speed than others by  $\sim$ 12 $\times$  while consuming reasonable parameters and computational operations. These results reveal the significant accuracy of our ESP-MedSAM-S on diverse medical segmentation tasks without demanding manual annotations.

### C. Comparison with State-of-the-Art PEFT and End-to-End SAMs

To perform the comprehensive evaluation of our ESP-MedSAM architecture. We take  $f_{ViT-Med}$ , SPPG and QDMD to construct ESP-MedSAM-T and further conduct comparisons on medical image segmentation with advanced PEFT SAMs [17]–[19], [42] and end-to-end SAMs [26]–[28]. As presented in Table II, ESP-MedSAM-T achieves average Dice of 89.07%, 96.64%, 80.93%, 93.14%, 88.08% and 92.03% on six medical imaging modalities, which performs better than current PEFT-based architectures with the manual point prompt mode and end-to-end SAMs. Remarkably, our ESP-MedSAM framework significantly reduces HD values by at least 20.02% in Colonoscopy, Ultrasound and Microscopy modalities. On the other hand, compared to existing lightweight architectures in Table I, our distilled model reveals less performance degradation, which displays the effectiveness of the proposed MMDKD strategy. Overall, these results

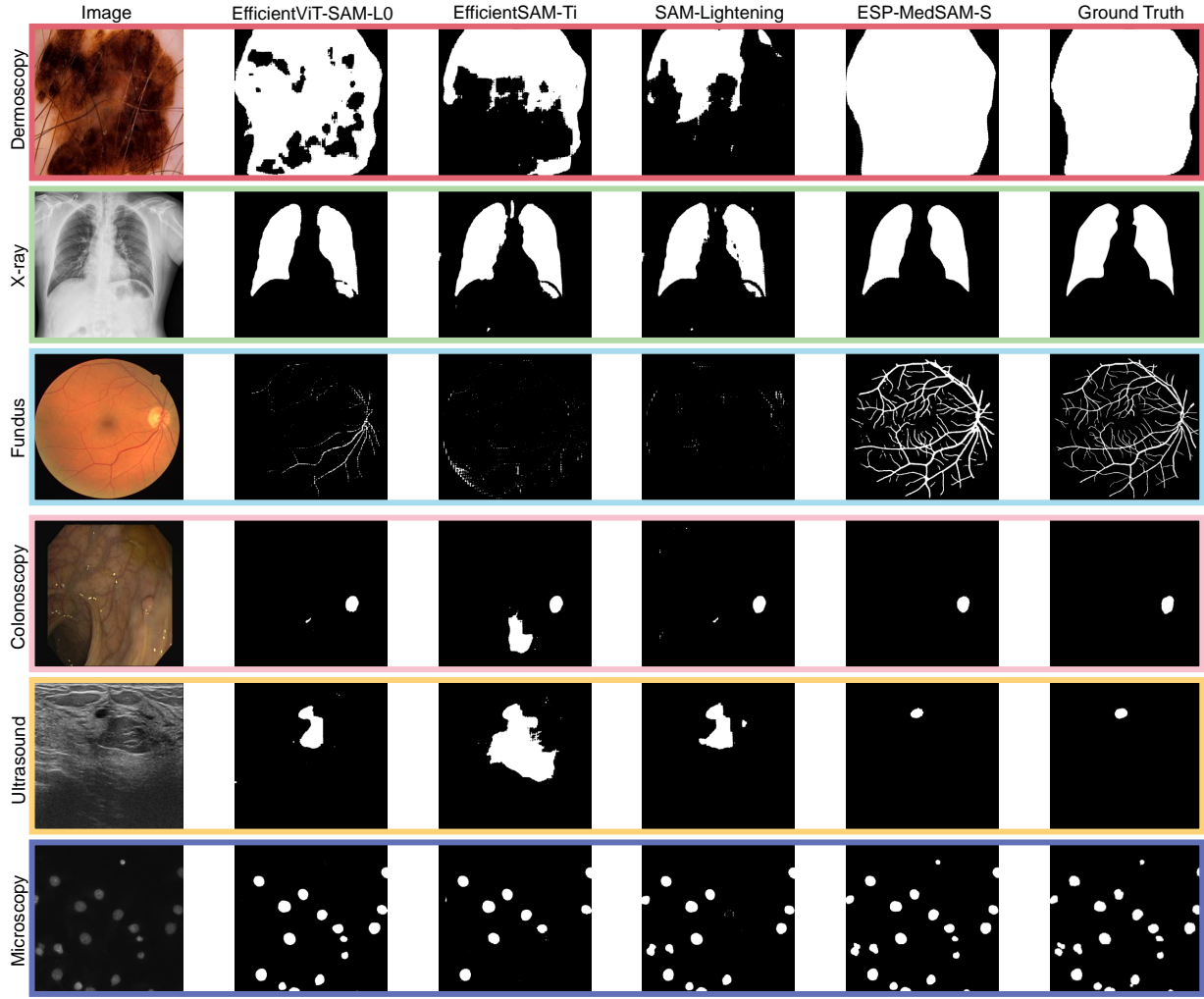


**Fig. 4.** Qualitative comparison with SOTA lightweight SAM frameworks with the automatic prompt generation mode on medical image segmentation over six modalities.

demonstrate the superior generalisation-efficiency trade-offs of our ESP-MedSAM-T as the teacher model on different medical modalities.

#### D. Comparison on Zero-shot Generalisation

We further evaluate the zero-shot generalisation of our ESP-MedSAM framework by comparing it with both foundation models and lightweight architectures on the STARE [43] dataset. In Table IV, we observe that our ESP-MedSAM-S achieves the best performance among all lightweight baselines, with the overwhelming Dice of 71.25% and HD of 88.00. Moreover, compared to the SOTA medical foundation models, our ESP-MedSAM-T also illustrates superior performance. In particular, our proposed model does not require manual annotations as prompts. These results demonstrate that our ESP-MedSAM has robust zero-shot generalisation capability and is more clinical-friendly to be applied in practical scenarios.

#### E. Comparison on Modality Transfer

We investigate the ability of our framework when transferred to other medical imaging modalities, such as

Histopathology, for nuclei image segmentation. To evaluate the performance, we compare ESP-MedSAM-S with all SOTA lightweight architectures, including U-Net series [3], [6], [53], [54], on the TNBC [52] dataset. As shown in Table V, some lightweight SAMs, based on manual point prompts, are inferior to traditional U-shape architectures [6], [54]. In contrast, our ESP-MedSAM-S framework, without the demand of manual prompts, outperforms these approaches with the best average Dice of 83.14% and HD of 111.83. These results reveal that ESP-MedSAM-S has better transfer capabilities when facing new modalities.

#### F. Ablation Study

To investigate the effectiveness of MMDKD, SPPG and QDMD modules, we further conduct a comprehensive ablation study on six medical imaging modalities, displayed in Table VI. By removing the devised modules from ESP-MedSAM, in 1<sup>st</sup> row, the fined-tuned SAM [35] (in Table II) serves as the ablation baseline. By separately adding the MMDKD (2<sup>nd</sup> row), SPPG (3<sup>rd</sup> row) and QDMD (4<sup>th</sup> row), the performance is increased with the average Dice of all modalities gain of 1.94%, 0.16%, 1.12%, respectively. Particularly, the MMDKD

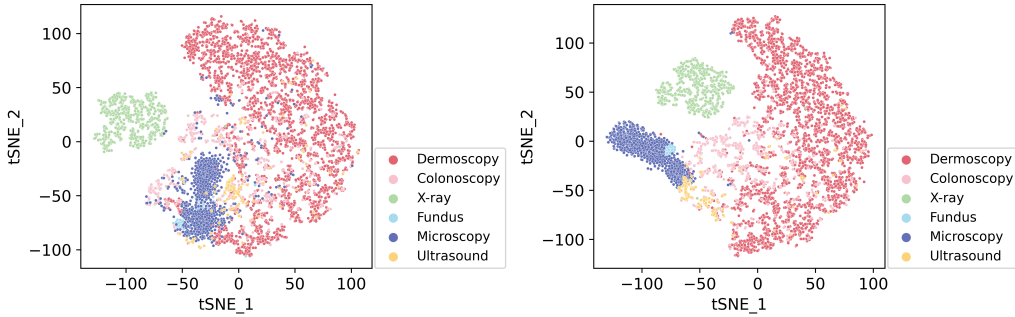


Fig. 5. Feature comparison via T-SNE between the baseline model and our ESP-MedSAM-S framework.

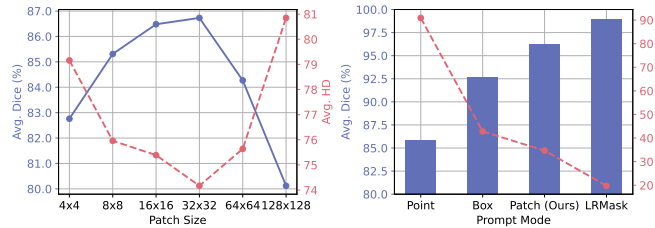


Fig. 6. Hyper-parameter analysis of patch size (left) and comparison of model performance based on different prompt types (right). Each prompt type utilises manual annotations (ground truth) as the input.

strategy decreases 67.90% of the parameters compared to SAM. The introducing SPPG module (3<sup>rd</sup> row) significantly reduces HD by 19.28%, which is more efficient than manual point prompts. The 5<sup>th</sup> row to the 7<sup>th</sup> row indicates the compatibility between each module. Overall, these ablation experiments prove that the MMDKD strategy significantly decreases the computation costs of ESP-MedSAM. SPPG eliminates the requirement for manual annotations. QDMD enhances the generalisation capabilities of the model across diverse modalities.

## G. Discussion

1) **Effectiveness of Patch Prompt Learning:** In this section, we delve into the rationale behind the adoption of the patch prompt learning strategy. Initially, we examine the performance of ESP-MedSAM-S based on SPPG with varying patch sizes. As illustrated in Fig. 6 (left), setting a larger patch size proves beneficial for the patch category task, albeit it provides less semantic information as prompts. Conversely, reducing the patch size increases the classification difficulty, consequently leading to more errors or noise. Additionally, we conduct a comparison of our devised patch prompt with point, box and Low-Resolution (LR) mask prompt modes in Fig. 6 (right). Considering that automatic prompt generation aims to learn the representation of human annotations, all prompt types utilize manual annotations (ground truth) as inputs for the experiment. Observations reveal that the manual patch prompt outperforms both the box and point prompts. Therefore, the learning patch prompt approach proves more efficient for guiding the segmentation decoding.

2) **Significance of Decoupling Strategy:** In the design of the MMDKD strategy, we adopt a decoupling strategy to

provide an independent encoding workflow for each modality. To qualitatively evaluate the efficiency of ESP-MedSAM-S in learning discriminative representations, we make a feature comparison via T-SNE with the baseline (the EfficientViT-SAM-L0 [40] in Table I). As shown in Fig. 5, the features produced by our method exhibits significant discriminability over the six medical image modalities, which benefits the following decoder in terms of segmentation masks significantly.

## V. CONCLUSION

In this paper, we have proposed the ESP-MedSAM framework for universal medical image segmentation. Specifically, The MMDKD strategy has been introduced to distil the knowledge from the foundation model to a lightweight image encoder and a modality controller. Then, SPPG has been devised to automatically produce a set of high-quality patch prompts for assisting segmentation decoding. Finally, QDMD has customised a specific segmentation workflow for each modality. Extensive experiments have demonstrated that ESP-MedSAM has lower computational complexity than the standard SAM and outperforms SOTA lightweight SAMs in diverse medical imaging segmentation tasks, exhibiting superior zero-shot generalisation and modality transfer ability.

## REFERENCES

- [1] I. Qureshi, J. Yan, Q. Abbas, K. Shaheed, A. B. Riaz, A. Wahid, M. W. J. Khan, and P. Szczuko, “Medical image segmentation using deep semantic-based methods: A review of techniques, applications and emerging trends,” *Inf. Fusion*, vol. 90, pp. 316–352, 2023.
- [2] G. Litjens, T. Kooi, B. E. Bejnordi, A. A. A. Setio, F. Ciompi, M. Ghafoorian, J. A. Van Der Laak, B. Van Ginneken, and C. I. Sánchez, “A survey on deep learning in medical image analysis,” *Med. Image Anal.*, vol. 42, pp. 60–88, 2017.
- [3] O. Ronneberger, P. Fischer, and T. Brox, “U-net: Convolutional networks for biomedical image segmentation,” in *MICCAI*. Springer, 2015, pp. 234–241.
- [4] J. Schlemper, O. Oktay, M. Schaap, M. Heinrich, B. Kainz, B. Glocker, and D. Rueckert, “Attention gated networks: Learning to leverage salient regions in medical images,” *Med. Image Anal.*, vol. 53, pp. 197–207, 2019.
- [5] A. Chakravarty and J. Sivaswamy, “Race-net: a recurrent neural network for biomedical image segmentation,” *IEEE J. Biomed. Health Inform.*, vol. 23, no. 3, pp. 1151–1162, 2018.
- [6] F. Isensee, P. F. Jaeger, S. A. Kohl, J. Petersen, and K. H. Maier-Hein, “nnu-net: a self-configuring method for deep learning-based biomedical image segmentation,” *Nature Methods*, vol. 18, no. 2, pp. 203–211, 2021.
- [7] H. Cao, Y. Wang, J. Chen, D. Jiang, X. Zhang, Q. Tian, and M. Wang, “Swin-unet: Unet-like pure transformer for medical image segmentation,” in *ECCV*. Springer, 2022, pp. 205–218.

[8] L. Sun, C. Li, X. Ding, Y. Huang, Z. Chen, G. Wang, Y. Yu, and J. Paisley, "Few-shot medical image segmentation using a global correlation network with discriminative embedding," *Comput. Biol. Med.*, vol. 140, p. 105067, 2022.

[9] C. Li, W. Ma, L. Sun, X. Ding, Y. Huang, G. Wang, and Y. Yu, "Hierarchical deep network with uncertainty-aware semi-supervised learning for vessel segmentation," *Neural Comput. Appl.*, pp. 1–14.

[10] C. Li, Y. Zhang, Z. Liang, W. Ma, Y. Huang, and X. Ding, "Consistent posterior distributions under vessel-mixing: a regularization for cross-domain retinal artery/vein classification," in *ICIP*. IEEE, 2021, pp. 61–65.

[11] C. Li, Y. Zhang, J. Li, Y. Huang, and X. Ding, "Unsupervised anomaly segmentation using image-semantic cycle translation," *arXiv preprint arXiv:2103.09094*, 2021.

[12] Z. Ding, Q. Dong, H. Xu, C. Li, X. Ding, and Y. Huang, "Unsupervised anomaly segmentation for brain lesions using dual semantic-manifold reconstruction," in *NeurIPS*. Springer, 2022, pp. 133–144.

[13] A. Dosovitskiy, L. Beyer, A. Kolesnikov, D. Weissenborn, X. Zhai, T. Unterthiner, M. Dehghani, M. Minderer, G. Heigold, S. Gelly *et al.*, "An image is worth 16x16 words: Transformers for image recognition at scale," in *ICLR*, 2020.

[14] A. Kirillov, E. Mintun, N. Ravi, H. Mao, C. Rolland, L. Gustafson, T. Xiao, S. Whitehead, A. C. Berg, W.-Y. Lo, P. Dollar, and R. Girshick, "Segment anything," in *ICCV*, October 2023, pp. 4015–4026.

[15] Y. Huang, X. Yang, L. Liu, H. Zhou, A. Chang, X. Zhou, R. Chen, J. Yu, J. Chen, C. Chen *et al.*, "Segment anything model for medical images?" *Med. Image Anal.*, vol. 92, p. 103061, 2024.

[16] J. Ma, Y. He, F. Li, L. Han, C. You, and B. Wang, "Segment anything in medical images," *Nature Communications*, vol. 15, no. 1, p. 654, 2024.

[17] X. Lin, Y. Xiang, L. Zhang, X. Yang, Z. Yan, and L. Yu, "Samus: Adapting segment anything model for clinically-friendly and generalizable ultrasound image segmentation," *arXiv preprint arXiv:2309.06824*, 2023.

[18] J. Wu, W. Ji, Y. Liu, H. Fu, M. Xu, Y. Xu, and Y. Jin, "Medical sam adapter: Adapting segment anything model for medical image segmentation," *arXiv preprint arXiv:2304.12620*, 2023.

[19] K. Zhang and D. Liu, "Customized segment anything model for medical image segmentation," *arXiv preprint arXiv:2304.13785*, 2023.

[20] N. Houlsby, A. Giurgiu, S. Jastrzebski, B. Morrone, Q. De Laroussilhe, A. Gesmundo, M. Attariyan, and S. Gelly, "Parameter-efficient transfer learning for nlp," in *ICML*. PMLR, 2019, pp. 2790–2799.

[21] J. Cheng, Y. Ye, Z. Deng, J. Chen, T. Li, H. Wang, Y. Su, Z. Huang, J. Chen, L. Jiang *et al.*, "Sam-med2d," *arXiv preprint arXiv:2308.16184*, 2023.

[22] E. J. Hu, Y. Shen, P. Wallis, Z. Allen-Zhu, Y. Li, S. Wang, L. Wang, and W. Chen, "LoRA: Low-rank adaptation of large language models," in *ICLR*, 2022.

[23] Z. Zhong, Z. Tang, T. He, H. Fang, and C. Yuan, "Convolution meets lora: Parameter efficient finetuning for segment anything model," in *ICLR*, 2024.

[24] M. A. Mazurowski, H. Dong, H. Gu, J. Yang, N. Konz, and Y. Zhang, "Segment anything model for medical image analysis: an experimental study," *Med. Image Anal.*, vol. 89, p. 102918, 2023.

[25] Q. Xu, W. Kuang, Z. Zhang, X. Bao, H. Chen, and W. Duan, "Sppnet: A single-point prompt network for nuclei image segmentation," in *MICCAI Workshop on MLMI*. Springer, 2023, pp. 227–236.

[26] X. Zhang, Y. Liu, Y. Lin, Q. Liao, and Y. Li, "Uv-sam: Adapting segment anything model for urban village identification," in *AAAI*, vol. 38, no. 20, 2024, pp. 22520–22528.

[27] Z. Cheng, Q. Wei, H. Zhu, Y. Wang, L. Qu, W. Shao, and Y. Zhou, "Unleashing the potential of sam for medical adaptation via hierarchical decoding," *CVPR*, 2024.

[28] Y. Gu, Q. Wu, H. Tang, X. Mai, H. Shu, B. Li, and Y. Chen, "Lesam: Adapt segment anything model for medical lesion segmentation," *IEEE J. Biomed. Health Inform.*, 2024.

[29] G. Hinton, O. Vinyals, and J. Dean, "Distilling the knowledge in a neural network," *arXiv preprint arXiv:1503.02531*, 2015.

[30] J. Yang, B. Martinez, A. Bulat, and G. Tzimiropoulos, "Knowledge distillation via softmax regression representation learning," in *ICLR*, 2020.

[31] B. Zhao, Q. Cui, R. Song, Y. Qiu, and J. Liang, "Decoupled knowledge distillation," in *CVPR*, 2022, pp. 11953–11962.

[32] D. Qin, J.-J. Bu, Z. Liu, X. Shen, S. Zhou, J.-J. Gu, Z.-H. Wang, L. Wu, and H.-F. Dai, "Efficient medical image segmentation based on knowledge distillation," *IEEE Trans. Med. Imaging*, vol. 40, no. 12, pp. 3820–3831, 2021.

[33] Q. Zhao, L. Zhong, J. Xiao, J. Zhang, Y. Chen, W. Liao, S. Zhang, and G. Wang, "Efficient multi-organ segmentation from 3d abdominal ct images with lightweight network and knowledge distillation," *IEEE Trans. Med. Imaging*, 2023.

[34] H. Wu, Z. Wang, Z. Zhao, C. Chen, and J. Qin, "Continual nuclei segmentation via prototype-wise relation distillation and contrastive learning," *IEEE Trans. Med. Imaging*, 2023.

[35] C. Zhang, D. Han, Y. Qiao, J. U. Kim, S.-H. Bae, S. Lee, and C. S. Hong, "Faster segment anything: Towards lightweight sam for mobile applications," *arXiv preprint arXiv:2306.14289*, 2023.

[36] K. Wu, J. Zhang, H. Peng, M. Liu, B. Xiao, J. Fu, and L. Yuan, "Tinyvit: Fast pretraining distillation for small vision transformers," in *ECCV*. Springer, 2022, pp. 68–85.

[37] C. Zhou, X. Li, C. C. Loy, and B. Dai, "Edgesam: Prompt-in-the-loop distillation for on-device deployment of sam," *arXiv preprint arXiv:2312.06660*, 2023.

[38] Y. Xiong, B. Varadarajan, L. Wu, X. Xiang, F. Xiao, C. Zhu, X. Dai, D. Wang, F. Sun, F. Iandola *et al.*, "Efficientsam: Leveraged masked image pretraining for efficient segment anything," *CVPR*, 2024.

[39] A. Wang, H. Chen, Z. Lin, J. Han, and G. Ding, "Repvit-sam: Towards real-time segmenting anything," *CVPR*, 2024.

[40] Z. Zhang, H. Cai, and S. Han, "Efficientvit-sam: Accelerated segment anything model without performance loss," *arXiv preprint arXiv:2402.05008*, 2024.

[41] Y. Songa, B. Pua, P. Wang, H. Jiang, D. Donga, and Y. Shen, "Sam-lightening: A lightweight segment anything model with dilated flash attention to achieve 30 times acceleration," *arXiv preprint arXiv:2403.09195*, 2024.

[42] Z. Zhong, Z. Tang, T. He, H. Fang, and C. Yuan, "Convolution meets lora: Parameter efficient finetuning for segment anything model," in *ICLR*, 2024.

[43] A. Hoover, V. Kouznetsova, and M. Goldbaum, "Locating blood vessels in retinal images by piecewise threshold probing of a matched filter response," *IEEE Trans. Med. Imaging*, vol. 19, no. 3, pp. 203–210, 2000.

[44] P. Tschandl, C. Rosendahl, and H. Kittler, "The ham10000 dataset, a large collection of multi-source dermatoscopic images of common pigmented skin lesions," *Sci. Data*, vol. 5, no. 1, pp. 1–9, 2018.

[45] N. Codella, V. Rotemberg, P. Tschandl, M. E. Celebi, S. Dusza, D. Gutman, B. Helba, A. Kalloo, K. Liopyris, M. Marchetti *et al.*, "Skin lesion analysis toward melanoma detection 2018: A challenge hosted by the international skin imaging collaboration (isic)," *arXiv preprint arXiv:1902.03368*, 2019.

[46] S. Candemir, S. Jaeger, K. Palaniappan, J. P. Musco, R. K. Singh, Z. Xue, A. Karargyris, S. Antani, G. Thoma, and C. J. McDonald, "Lung segmentation in chest radiographs using anatomical atlases with nonrigid registration," *IEEE Trans. Med. Imaging*, vol. 33, no. 2, pp. 577–590, 2013.

[47] S. Jaeger, A. Karargyris, S. Candemir, L. Folio, J. Siegelman, F. Callaghan, Z. Xue, K. Palaniappan, R. K. Singh, S. Antani *et al.*, "Automatic tuberculosis screening using chest radiographs," *IEEE Trans. Med. Imaging*, vol. 33, no. 2, pp. 233–245, 2013.

[48] J. Staal, M. D. Abràmoff, M. Niemeijer, M. A. Viergever, and B. Van Ginneken, "Ridge-based vessel segmentation in color images of the retina," *IEEE Trans. Med. Imaging*, vol. 23, no. 4, pp. 501–509, 2004.

[49] J. Bernal, F. J. Sánchez, G. Fernández-Esparrach, D. Gil, C. Rodríguez, and F. Vilariño, "Wm-dova maps for accurate polyp highlighting in colonoscopy: Validation vs. saliency maps from physicians," *Comput. Med. Imaging Graph.*, vol. 43, pp. 99–111, 2015.

[50] M. H. Yap, G. Pons, J. Martí, S. Ganau, M. Sentis, R. Zwiggelaar, A. K. Davison, and R. Martí, "Automated breast ultrasound lesions detection using convolutional neural networks," *IEEE J. Biomed. Health Inform.*, vol. 22, no. 4, pp. 1218–1226, 2017.

[51] J. C. Caicedo, A. Goodman, K. W. Karhohs, B. A. Cimini, J. Ackerman, M. Haghghi, C. Heng, T. Becker, M. Doan, C. McQuin *et al.*, "Nucleus segmentation across imaging experiments: the 2018 data science bowl," *Nature Methods*, vol. 16, no. 12, pp. 1247–1253, 2019.

[52] P. Naylor, M. Laé, F. Reyal, and T. Walter, "Segmentation of nuclei in histopathology images by deep regression of the distance map," *IEEE Trans. Med. Imaging*, vol. 38, no. 2, pp. 448–459, 2018.

[53] J. Chen, Y. Lu, Q. Yu, X. Luo, E. Adeli, Y. Wang, L. Lu, A. L. Yuille, and Y. Zhou, "Transunet: Transformers make strong encoders for medical image segmentation," *arXiv preprint arXiv:2102.04306*, 2021.

[54] N. Ibtehaz and D. Kihara, "Acc-unet: A completely convolutional unet model for the 2020s," in *MICCAI*. Springer, 2023, pp. 692–702.